Migration with surface and internal multiples

Shang Huang and Daniel O. Trad

ABSTRACT

Multiples can provide additional information for subsurface structures compared with primary reflections. In this paper, we consider two different uses of multiples for imaging. First, we will look at the use of the first-order surface multiples for reverse time migration (RTM). Observed primaries are extracted from shot records and injected as virtual sources and surface multiples are used as data and back-propagated in time. Then the cross-correlation between primary wave and the first-order surface multiple is used as image condition. RTM of surface multiples gives a more extensive illumination than RTM of primaries. In addition, least-squares reverse time migration (LSRTM) of surface multiples presents improved vertical resolution compared with RTM. Also, LSRTM of the first-order surface multiple can recover the information from upper-side dipping events as well as some small flanks. The main requirement of these benefits is, however, quite challenging: to achieve multiple separation before migration.

The second use of multiples we examine here is full-wavefield migration (FWM). This method uses an inversion-based approach to update the subsurface image. Reflection coefficient updates are obtained from scattering effects, including reflections and differential transmissions. A horizontal-layered model is used for proving the benefits of using FWM. Forward modeling by phase shift plus interpolation derives stable downgoing and upgoing wavefields separately, which can predict primary, surface multiples and internal multiples in a full-wavefield response. FWM of total wavefields can provide more details in the image compared with FWM of primary only. Adding energy from multiples into migration is not a replacement for migrating primary reflections, but it can be a useful complement to improve the image resolution and illumination for an accurate geological interpretation.

INTRODUCTION

In seismic exploration, traditionally, multiple reflections are considered as noise and removed as much as possible before imaging. However, multiples can provide valuable information about the subsurface structure. Multiple reflections are distinguished from primary waves in that seismic events have more than one reflection between source and receiver (Sengbush, 1983). Since multiples travel long distances, they can illuminate a broader subsurface region where the primary reflection might not illuminate well due to limited aperture. Also, multiples have smaller reflection angles than primaries (Snieder, 2002) and are sensitive to small time-lapse changes for the medium. Thus, multiples information is an asset for imaging methods.

Migration is a process that re-locates the seismic events to the true space or time location. Migration of multiples becomes a helpful implement to mitigate the wrong interpretation of dipping structures or lateral velocity variation. In the past, surface-related multiples have been used for shot-record migration (Berkhout and Verschuur, 1994; Verschuur and Berkhout, 2011; Guitton, 2002) to improve the subsurface reflectors image quality. These methods consider the subsurface structure is illuminated from primary reflections and sec-

ondary source energy (multiple reflections). The methods mentioned above use "WRW" model (Berkhout and Verschuur, 1994) to perform primary and multiple wave extrapolation. Verschuur and Berkhout (2015) came up with a closed-loop approach to migrate both internal and surface multiples. Full-wavefield migration (Berkhout and Verschuur, 2016; Davydenko and Verschuur, 2017) including all orders of multiples has been proposed as a means to enhance image illumination and resolution.

Besides full wavefield migration, reverse time migration can migrate surface multiples as well. Reverse time migration (RTM) (Baysal et al., 1983) is given by a forward and reverse time propagation of source and receiver wavefields respectively, followed by an imaging condition. It can handle steep dip angles and adapts to any velocity variations. Liu et al. (2011) applied reverse time migration to migrate all-order multiples. Zhang and Schuster (2013), and Liu et al. (2016), used least-squares reverse time migration (LSRTM) for controlled-order multiples, since higher-order multiples amplitude is quite smaller than the first- and second-order multiple. Least-squares full-wavefield migration (Lu et al., 2018) based on separated-wavefield imaging can jointly image both primary and high-order reflected energy.

RTM and LSRTM can handle surface multiples well but has more difficulties to use internal multiples because of the crosstalk between them. FWM not only can predict surface multiples, but also will generate and use internal multiples better compared with RTM, because FWM provides some internal control mechanism on which internal multiples to use. In this paper, we will try the application of RTM and LSRTM for surface multiples and FWM for migrating total wavefields including primary, surface and internal multiples. This paper is divided into four sections. The introduction gives an overview of different migration approaches with multiples. The theory section demonstrates reverse time migration (RTM), least-squares reverse time migration (LSRTM) and full-wavefield migration (FWM) in detail, followed by the results for applying the three methods above. The final section presents future work and conclusion.

THEORY

Reverse time migration (RTM) with surface multiples

In this experiment, we try RTM of surface multiples to test the illumination improvements for a migrated image. In the workflow in Figure 1 and Figure 2, we show how we use primaries (blue lines in Figure 2) as virtual sources instead of a source wavelet. As a benefit, there is no need to estimate the source wavelet required in the usual migration process. Shots on the surface generate simultaneous primary wavefields that propagate downward into the subsurface. The second step in the workflow is to backward extrapolate the first-order surface multiple (red lines in Figure 2). These can be separated from data by filtering with Radon transform, wavefield separation, or other standard methods. The surface multiples are back-propagated as the reversed-time receiver wavefields. The third step is to implement cross-correlation imaging condition shown in equation (1) (Liu et al., 2011),

$$\mathrm{Image}(x,z) = \sum_{t=1}^{t_{max}} P_F(x,z,t) * M_B(x,z,t) \tag{1}$$

where P_F is forward primary or forward zero-th order multiple, M_B is back-propagated first-order surface multiple. RTM of surface multiples only gives an artifact-free image when the forward-propagated $(N-1)$th-order multiple cross-correlated with the back-propagated Nth-order multiple. Otherwise, crosstalk invoked from cross-correlation with different orders of multiples will appear on the image.

Least-squares reverse time migration (LSRTM) with surface multiples

To improve image resolution and suppress artifacts, we use least-squares reverse time migration which updates the reflectivity coefficients iteratively to the point where they can predict the observed data up to reasonable error. We apply L2 norm objective function for LSRTM with surface multiples (Zhang and Schuster, 2013)

$$f(\mathbf{m}) = \frac{1}{2}||\mathbf{Lm} - \mathbf{M}||^2 \tag{2}$$

where $\mathbf{L}$ denotes the forward modeling operator for generating multiples, $\mathbf{m}$ presents the reflectivity model, and $\mathbf{M}$ means observed surface multiples. The gradient of this objective function is

$$\mathbf{g} = \mathbf{L}^T[\mathbf{Lm} - \mathbf{M}] = \mathbf{L}^T\Delta\mathbf{d} \tag{3}$$

where $\Delta\mathbf{d}$ is the difference between predicted and observed multiple data. Compared with Zhang and Schuster (2013), we use a conjugate gradient method to update the reflectivity coefficient in an efficient convergence rate,

$$\alpha_k = \frac{\mathbf{g}_k^T\mathbf{g}_k}{(\mathbf{Lg}_k)^T(\mathbf{Lg}_k)} \tag{4}$$

$$\mathbf{m}_{k+1} = \mathbf{m}_k + \alpha_k\mathbf{g}_k \tag{5}$$

$$\mathbf{g}_{k+1} = \mathbf{g}_k - \alpha_k\mathbf{Lg}_k \tag{6}$$

$$\beta_k = \frac{\mathbf{g}_{k+1}^T\mathbf{g}_{k+1}}{\mathbf{g}_k^T\mathbf{g}_k} \tag{7}$$

$$\mathbf{g}_{k+1} = \mathbf{g}_{k+1} + \beta_k\mathbf{g}_k \tag{8}$$

where k is the iteration number. The step size α is given by the energy of migration residual divided by the energy of prediction residual. The other step size β is the dot product of updated gradient divided by the dot product of previous gradient. If the data residual is smaller than a threshold or the number of iterations meet with the maximum limit, the updating procedure will stop.

Full-wavefield migration (FWM) with surface and internal multiples

1. Phase shift plus interpolation

Zero-offset pressure data based wavefield extrapolation (Gazdag and Sguazzero, 1984), in the (x,t) domain, satisfies the 2-D scalar wave equation

$$\frac{\partial^2 p(x,z,t)}{\partial z^2} = \frac{1}{v^2}\frac{\partial^2 p(x,z,t)}{\partial t^2} - \frac{\partial^2 p(x,z,t)}{\partial x^2}, \tag{9}$$

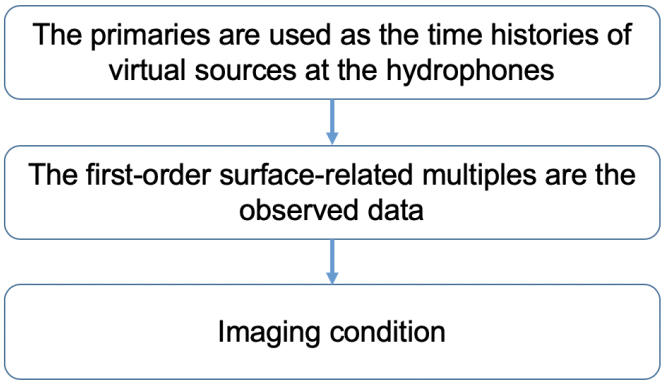

FIG. 1: Workflow for RTM with multiples

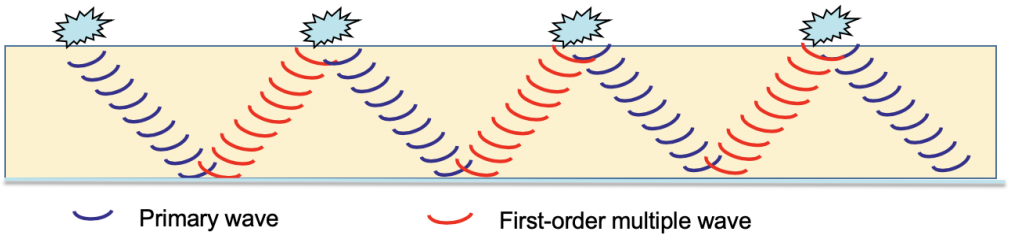

FIG. 2: Forward and backward wave propagation in RTM with surface multiple

where x represents the midpoint, z means depth, t is the two-way traveltime, and v denotes the half velocity. Wavefield extrapolation can be expressed by the sum of a double Fourier series in the frequency and wavenumber domain

$$p(x,z,t) = \sum_{k_x}\sum_{\omega} P(k_x,z,\omega)\exp[i(k_x x + \omega t)], \tag{10}$$

where k_x is the midpoint wavenumber and ω is the temporal frequency. Substitute equation 10 into equation 9, the wave equation will be

$$\frac{\partial^2 P}{\partial z^2} = -(\frac{\omega^2}{v^2} - {k_x}^2)P = -{k_z}^2 P, \tag{11}$$

where $k_z = \pm\frac{\omega}{v}[1-(\frac{vk_x}{\omega})^2]^{1/2}$. One analytic solution to equation 11 is

$$P(k_x, z+\Delta z, \omega) = P(k_x, z, \omega)\exp(ik_z\Delta z), \tag{12}$$

which is associated with Rayleigh II integral (Berkhout et al., 1999) using dipoles on the surface to reconstruct the pressure field in the lower half-space. Equation 12 means that the neighbouring layer wavefield is derived by current level wavefield times an exponential operator related to the interval depth. If k_z and ω have different signs, the wavefield will propagate in the positive time direction. On the other hand, wave would propagate in the reverse time direction if they share the same sign. Since simulating the recorded seismic data to perform downward or upward wave propagation is an inverse process, k_z and ω should have sign agreement

$$k_z = \frac{\omega}{v}[1-(\frac{vk_x}{\omega})^2]^{1/2}, \tag{13}$$

We assume positive sign of Δz in equation 12 means downward extrapolation direction, and negative sign denotes upward direction. Substituting equation 13 into equation 12, we can determine the downward wave extrapolation equation for constant velocity in frequency-wavenumber domain

$$P(k_x, z+\Delta z, \omega) = P(k_x, z, \omega)\exp\{i\frac{\omega}{v}[1-(\frac{vk_x}{\omega})^2]^{1/2}\Delta z\}, \tag{14}$$

According to equation 14, the wavefield extrapolation operator is defined as

$$\mathbf{W} = \exp\{i\frac{\omega}{v}[1-(\frac{vk_x}{\omega})^2]^{1/2}\Delta z\}, \tag{15}$$

The smoothed background velocity model will yield inaccurate extrapolator in frequency wavenumber domain. To calculate accurate and stable wavefields under the horizontal layered model assumption, we apply phase shift plus interpolation (PSPI) (Gazdag and Sguazzero, 1984). The PSPI method originally uses two or more reference velocities ($v_1 = Min[v(x,z)]$ and $v_2 = Max[v(x,z)]$) to interpolate downward wavefields extrapolated by phase shift: $P_1(x, z\pm\Delta z, \omega)$ and $P_2(x, z\pm\Delta z, \omega)$. In this paper, we also apply PSPI for upward propagation wavefields. Phase-shifted wavefields $P_1(k_x, z\pm\Delta z, \omega)$ and $P_2(k_x, z\pm\Delta z, \omega)$ are in frequency wavenumber domain. To apply interpolation, we should do inverse Fourier transform for wavefields from f-kx domain to f-x domain, leading to the two reference wavefields P_1 and P_2

$$P_1(x, z\pm\Delta z, \omega) = A_1\exp(i\theta_1) \tag{16}$$

$$P_2(x, z\pm\Delta z, \omega) = A_2\exp(i\theta_2) \tag{17}$$

The interpolated amplitude and phase then can be decided by linear interpolation

$$A = \frac{A_1(v_2-v)+A_2(v-v_1)}{v_2-v_1} \tag{18}$$

$$\theta = \frac{\theta_1(v_2-v)+\theta_2(v-v_1)}{v_2-v_1} \tag{19}$$

So the wavefield after interpolation gives

$$P(x, z\pm\Delta z, \omega) = A\exp(i\theta) \tag{20}$$

2. Bremmer series

Before introducing the forward model in full-wavefield migration, we would like to illustrate the Bremmer series, because recursively forward modeling in full-wavefield migration is similar to this series. Bremmer (1951) applied the complete series including all the refractions and reflections generated from the discontinuity boundaries, as a solution to the differential equation in a discontinuous model.

$$u'' + k^2(x)u = 0, \tag{21}$$

where $k(x)$ in this method demonstrates a step-function, which can be interpreted as the propagation of a plane wave through a stratified medium.

A Bremmer series decomposition was developed by Atkinson (1960) such that waves $u(x)$ can be represented by the sum of two terms

$$u(x) = v(x) + w(x), \tag{22}$$

where $v(x)$ is the total contribution of all forward propagating waves which start below the point x, and $w(x)$ represents the total of all back-propagated waves starting above x.

Mendel (1978) used the Bremmer series to generating a complete response for the updated state equation model. In his method, one can apply superposition on the intersection point of the ray diagram (Figure 3), to obtain the reflected and transmitted signals

$$u_k(t+\tau_k) = r_k d_k^T(t-\tau_k) + (1-r_k)u_{k+1}(t) \quad (k = 0, 1, 2, ..., K-1), \tag{23}$$

$$d_{k+1}^T(t) = (1+r_k)d_k^T(t-\tau_k) - r_k u_{k+1}(t) \quad (k = 0, 1, 2, ..., K-1), \tag{24}$$

where symbols $u_k(t)$ and $d_k(t)$ denote the upgoing and downgoing waves at the kth layer, each layer is characterized by the one way travel time τ_k, and normal incidence reflection coefficients r_k. At the Kth interface, one assume $u_{K+1}(t) = 0$, because no source exists in the basement. Then the reflection and transmission from bottom can be derived

$$u_K(t+\tau_K) = r_K d_K^T(t-\tau_K) \tag{25}$$

$$d_{K+1}^T(t) = (1+r_K)d_K^T(t-\tau_K) \tag{26}$$

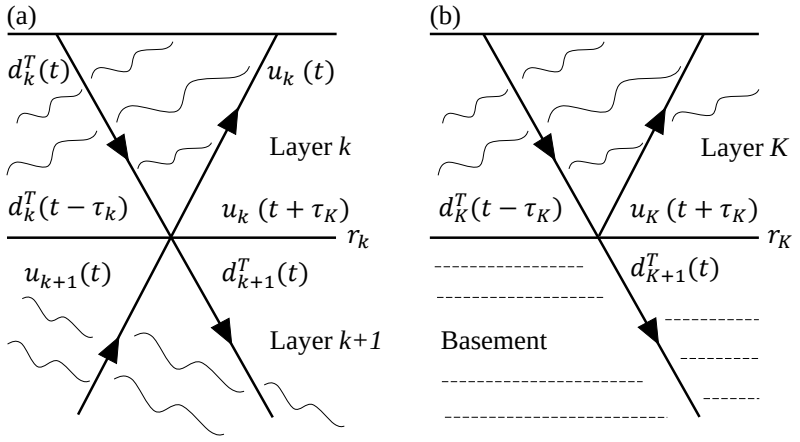

FIG. 3: Reflected and transmitted waves at (a) interface k and (b) interface K, adapted by Mendel (1978).

3. Forward model in full wavefield migration

Forward model in full wavefield migration (FWM) (Berkhout, 2014) (Davydenko and Verschuur, 2017) delineates incoming and outgoing wavefields in terms of approaching the subsurface grid point or not. At each depth level, wavefields approaching this depth

from above or below are defined as P and wavefields leaving this level from both sides are Q. Traditionally, a positive sign (+) represents the downward extrapolation and a negative sign (-) means the upward propagation. Outgoing wavefields $Q^-(z_m)$ include not only the reflection from incoming wavefields $P^+(z_m)$ above the same depth layer, but also the transmission from upgoing incoming wavefields $P^-(z_m)$ below the same level. Thus, the total outgoing wavefield from depth level z_m can be determined by the sum of reflection of incoming wavefield from the same side of layer and transmission of incoming wavefield from the opposite side of layer

$$\vec{Q}^+(z_m) = \vec{P}^+(z_m) + \delta\mathbf{T}^+(z_m)\vec{P}^+(z_m) + \mathbf{R}^\cap(z_m)\vec{P}^-(z_m), \tag{27}$$

$$\vec{Q}^-(z_m) = \vec{P}^-(z_m) + \delta\mathbf{T}^-(z_m)\vec{P}^-(z_m) + \mathbf{R}^\cup(z_m)\vec{P}^+(z_m), \tag{28}$$

where for the first two terms in equation 27 and 28 are the transmitted incoming wavefield where the transmission coefficient is $\mathrm{T} = \mathbf{I} + \delta\mathrm{T}$. $\mathrm{R}^\cap$ and $\mathrm{R}^\cup$ are the reflection operator from below and above one depth level. If the velocity distribution keeps the same at a depth level, reflectivity coefficient should be zero. In other words, a reflection wavefield only appears when the media has discontinuity variation.

For acoustic media, if there are small contrasts for shear-wave propagation velocity, $\delta\mathrm{T}^+$ and $\delta\mathrm{T}^-$ can be assumed as $\mathrm{R}^\cup$ and $\mathrm{R}^\cap$ respectively. In this paper, we start with considering the angle-independent case, so the reflection operator can be represented as a diagonal matrix consisting of frequency-independent scalar coefficients. The sketch of a wave propagation is shown in Figure 4. Equations 27 and 28 can be written as

$$\vec{Q}^+(z_m) = \vec{P}^+(z_m) + \mathbf{R}^\cup(z_m)\vec{P}^+(z_m) + \mathbf{R}^\cap(z_m)\vec{P}^-(z_m), \tag{29}$$

$$\vec{Q}^-(z_m) = \vec{P}^-(z_m) + \mathbf{R}^\cap(z_m)\vec{P}^-(z_m) + \mathbf{R}^\cup(z_m)\vec{P}^+(z_m), \tag{30}$$

where the two last terms in the above equations are equal. The two terms are determined as the secondary sources or scattering terms $\delta\vec{S}$ because they indicate the variation wavefields in both directions:

$$\delta\vec{S}(z_m) = \mathbf{R}^\cup(z_m)\vec{P}^+(z_m) + \mathbf{R}^\cap(z_m)\vec{P}^-(z_m), \tag{31}$$

After propagation, $Q^-(z_m)$ will become incoming wavefield $P^-(z_{m-1})$ at the neighbouring depth level z_{m-1}. The outgoing wavefield $Q^+(z_m)$ shares the same behaviour and becomes $P^+(z_{m+1})$ after extrapolation. Thus, we can obtain the equations for wave propagation between neighbouring layers

$$\vec{P}^+(z_m) = \mathbf{W}(z_m, z_{m-1})\vec{Q}^+(z_{m-1}), \tag{32}$$

$$\vec{P}^-(z_m) = \mathbf{W}(z_m, z_{m+1})\vec{Q}^-(z_{m+1}), \tag{33}$$

where $\mathrm{W}(z_m, z_{m\pm1})$ is a one-way wavefield extrapolation propagator, from neighbouring depth level $z_{m\pm1}$ to the current depth z_m. In this paper, $\mathrm{W}(z_m, z_{m\pm1})$ is calculated in the frequency wavenumber domain and only depends on the background velocity. Columns in $\mathrm{W}(z_m, z_{m\pm1})$ mean negative and positive wavenumber, rows denote the positive temporary frequency domain.

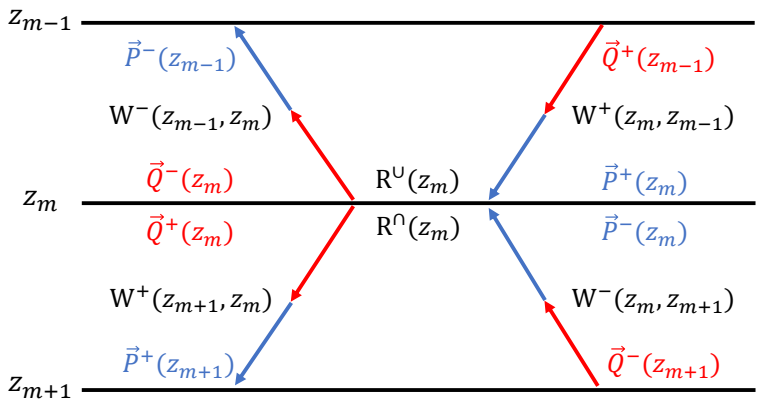

FIG. 4: Incoming wavefield (P) and outgoing wavefield (Q) generated at each gridpoint of depth level z_m. The outgoing wavefields will become incoming wavefields at the the neighbouring depth level after propagation. Adapted by Davydenko and Verschuur (2017)

The next step is to calculate downgoing wavefields and upgoing wavefields recursively for obtaining forward modeling. One downgoing and an upgoing term is defined as a wavefield round-trip. Recursive calculation means that for the second time calculating the downgoing propagation, this method will use previous downgoing and upgoing wavefields; so as the upgoing extrapolation.

The downward extrapolated wavefield can be determined by the accumulation of source on the surface and all secondary sources at subsurface:

$$\vec{P}^+(z_m) = \sum_{n<m} \mathbf{W}(z_m, z_n)[\vec{S}^+(z_n) + \delta\vec{S}(z_n)], \tag{34}$$

Then, substitute the downgoing wavefield into equation 31 to update the scattering terms. After that, upgoing wavefield can be calculated as

$$\vec{P}^-(z_m) = \sum_{n>m} \mathbf{W}(z_m, z_n)\delta\vec{S}(z_n), \tag{35}$$

For equation 34 and 35, traditionally we only consider the surface source $\vec{S}^+(z_0)$ is non-zero and all $\vec{S}^\pm$ at subsurface are zero.

When we have obtained the upward extrapolation, substitute equation 35 into equation 31 and update the scattering terms. Thus, for the next round-trip, the downgoing wavefields will include not only the source wavefield, but also the reflections of previous upgoing wavefields at each depth layer. Those reflections are also generating internal multiples between layers, which means that when the number of round-trips increases, a new order of surface multiples and internal multiples will be added in the propagation equations.

After generating the full wavefield (Figure 5), we can obtain the predicted data, then we can calculate the residual between predicted data and observed data. The residual is the input of the next imaging part in the algorithm.

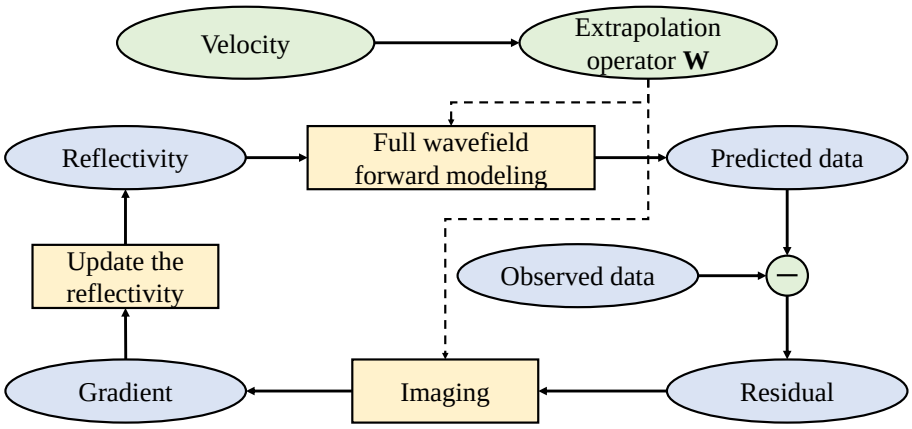

FIG. 5: Workflow for full wavefield migration (adapted from Davydenko and Vershuur (2017))

4. Imaging in full wavefield migration

Based on the workflow shown in the Figure 5, in the imaging process, full wavefield migration is trying to use data residual to update the reflectivity coefficient for each layer during the iterations. The objective function in FWM (Davydenko and Verschuur, 2017) is given:

$$J = \sum_{\omega} ||\Delta \mathbf{P}||_2^2 + f(\mathbf{R}) = \sum_{\omega} ||\mathbf{P}_{obs} - \mathbf{P}_{mod}||_2^2 + f(\mathbf{R}) \tag{36}$$

where P_{obs} means the observed data on the surface and P_{mod} is our predicted data and ΔP is the difference between the observed and modeled data. $f(\mathrm{R})$ denotes the regularization term. In this paper, we use Cauchy function criterion (Amundsen, 1991) as the regularization in the migration

$$f(\mathbf{R}(z_m)) = \frac{1}{2} \sum_{z_m} \ln(1 + \frac{\mathrm{diag}(\mathbf{R}(z_m))^H \mathrm{diag}(\mathbf{R}(z_m))}{\lambda^2}) \tag{37}$$

where H means the complex conjugate, and parameter λ corresponds to the scale parameter in the Cauchy distribution.

The gradients of the objective function with respect to the above and below reflectivity coefficients are obtained by:

$$\mathbf{C}^{\cup}(z_m) = [\Delta \mathbf{P}^{-}(z_m)][\mathbf{P}^{+}(z_m)]^H \tag{38}$$

$$\mathbf{C}^{\cap}(z_m) = [\Delta \mathbf{P}^{+}(z_m)][\mathbf{P}^{-}(z_m)]^H \tag{39}$$

$$\Delta \mathbf{P}^{-}(z_m) = [\mathbf{W}(z_0, z_m)]^H [\mathbf{P}_{obs}(z_0) - \mathbf{P}_{mod}(z_0)] \tag{40}$$

$$\Delta \mathbf{P}^{+}(z_m) = \sum_{n>m} [\mathbf{W}(z_n, z_m)]^H [\mathbf{R}^{\cup}(z_n)]^{-1} \Delta \mathbf{P}^{-}(z_n) \tag{41}$$

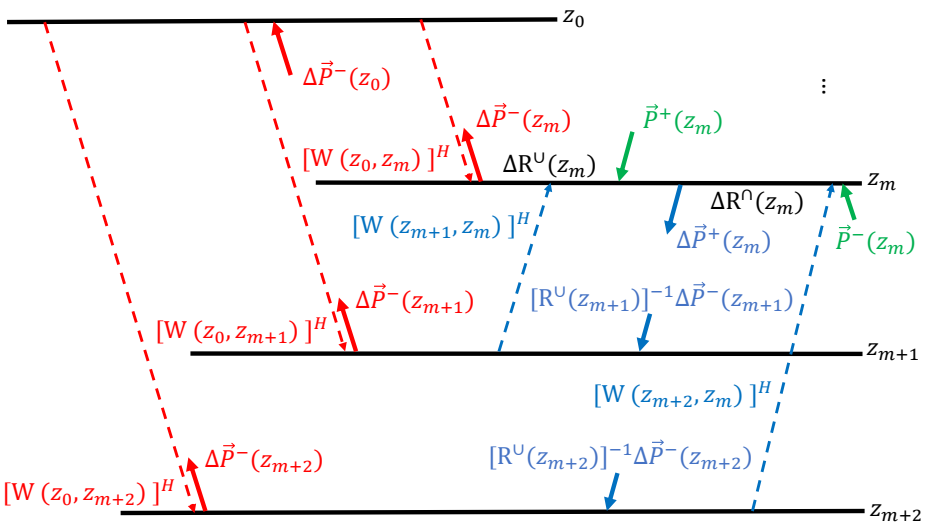

FIG. 6: Back-propagated residual (red solid lines) and reflected residual (blue solid lines). Reflectivity updates of both sides can be projected by the product of forward-modelled wavefield (green lines) and residuals.

where $\Delta\mathbf{P}^-(z_m)$ represents the back-propagated residual derived from the surface data residual $(\mathbf{P}_{obs}(z_0) - \mathbf{P}_{mod}(z_0))$. In Figure 6, surface data residual $\Delta\mathbf{P}^-(z_0)$ (red solid line) will propagate backward to different subsurface layers. At discontinuity boundaries, back-propagated residual will reflect and propagate upward by upgoing extrapolation operator. By summing over all the upward propagation of the reflected back-propagated residuals, we can obtain $\Delta\mathbf{P}^+(z_m)$ (blue solid line). At above depth level z_m, the gradient is the multiplication between $\Delta\mathbf{P}^-(z_m)$ (red solid line) and $\mathbf{P}^+(z_m)$ (green solid line). Gradient below the reflector is the multiplication of $\Delta\mathbf{P}^+(z_m)$ (blue solid line) and $\mathbf{P}^-(z_m)$ (green solid line).

For the imaging condition, one can sum over the frequency components of gradients which is corresponding to zero time cross-correlation imaging condition:

$$\Delta\mathbf{R}(z_m) = \mathrm{diag}(\sum_{\omega}\mathbf{C}(z_m)) + f'(\mathbf{R}(z_m)) \tag{42}$$

where the derivative of Cauchy criterion in terms of reflection coefficient should be

$$f'(\mathbf{R}(z_m)) = \frac{\mathrm{diag}(\mathbf{R}(z_m))}{1+\lambda^{-2}\mathrm{diag}(\mathbf{R}(z_m))^H\mathrm{diag}(\mathbf{R}(z_m))} \tag{43}$$

Next, we can update the reflectivity matrix as follow:

$$\mathbf{R}_i^{\cup}(z_m) = \mathbf{R}_{i-1}^{\cup}(z_m) + \alpha\Delta\mathbf{R}_{i-1}^{\cup}(z_m) \tag{44}$$

$$\mathbf{R}_i^{\cap}(z_m) = \mathbf{R}_{i-1}^{\cap}(z_m) + \beta\Delta\mathbf{R}_{i-1}^{\cap}(z_m) \tag{45}$$

where i denotes the current iteration number and α and β are determined by a line search method, Armijo rule

$$r(\mathbf{R}_{i+1}) \leq r(\mathbf{R}_i) + c_1\alpha_i\mathbf{C}_i^{\mathrm{T}}\mathbf{C}_i \tag{46}$$

where we regard $r(\mathbf{R}_{i+1})$ as the updated residual and $r(\mathbf{R}_i)$ as the previous iteration residual. If the condition satisfies equation 46, the step size α_i should decrease as $\alpha_i/2$. Normally, hyper-parameter c_1 is defined as 10^{-4}.

For the acoustic media, we can only estimate one-side reflectivity coefficient because $\mathbf{R}^{\cup} = -\mathbf{R}^{\cap}$.

NUMERICAL EXAMPLES

In this section, we show three numerical examples. We apply reverse time migration (RTM) on a horizontal-layered model and least-squares reverse time migration (LSRTM) on a three-reflector model, to demonstrate how migration of surface multiples extends reflector illumination. Then, we implement full-wavefield migration (FWM) on a simple acoustic flat model, to understand how internal multiples can improve the reflectors' resolution for migration.

Example 1: RTM of the first-order surface multiple in horizontal-layered model

The first example is a proof of concept that a first-order surface multiple can expand the illumination for migrating a horizontal layer. Horizontal distance for the true velocity model Figure 7 was 4808 meters, and the depth was 2000 meters. The upper layer velocity was 2000 m/s and the bottom layer velocity was 3000 m/s. Source and receivers were located at 40 meters depth. The receivers' spacing was set as 20 meters, while we only used one shot at the central horizontal location in this example. The recorded total time was 2.88 seconds with 0.0008 seconds as a time interval. Figure 7b is the smoothed background velocity model for migration.

We generated a primary and a first-order multiple using a convolutional model (Figure 8a and b). Then we applied RTM on the primary only (Figure 9a), resulting in migration with a small aperture. Since primary only reflects once at the reflector along its travel path, the reflection angle will approach the critical angle when the offset increases. For a large reflection angle, receivers cannot record the total time histories due to limited offset, which yields data loss and collapse in the migrated outcome. In Figure 9b, we show the result of RTM using the primary as the source and the multiple as data. The image has wider illumination as expected, precisely between offset 0-1000 meters and after 4000 meters. Also, the image shown in Figure 9b highlights fewer artifacts about the shot effect and improved vertical resolution compared with Figure 9a.

Example 2: LSRTM of the first-order surface multiple in three-reflector model

In this example, we test whether the first-order surface multiple migration can handle both dips and curvature. The model (Figure 10a) was discretized into a 501 $\times$ 501 grid with a spacing interval 10 meters. Velocity values varied from 1500 m/s to 3000 m/s. The receiver spacing was 20 meters and the shot was located at the center. Since multiple will travel longer time compared with primary, we set recorded time as 8.8 seconds with 0.0008 seconds time interval. In this case, we used finite-difference forward modeling to generate the data and then separated the primary from the multiple using a Radon transform and

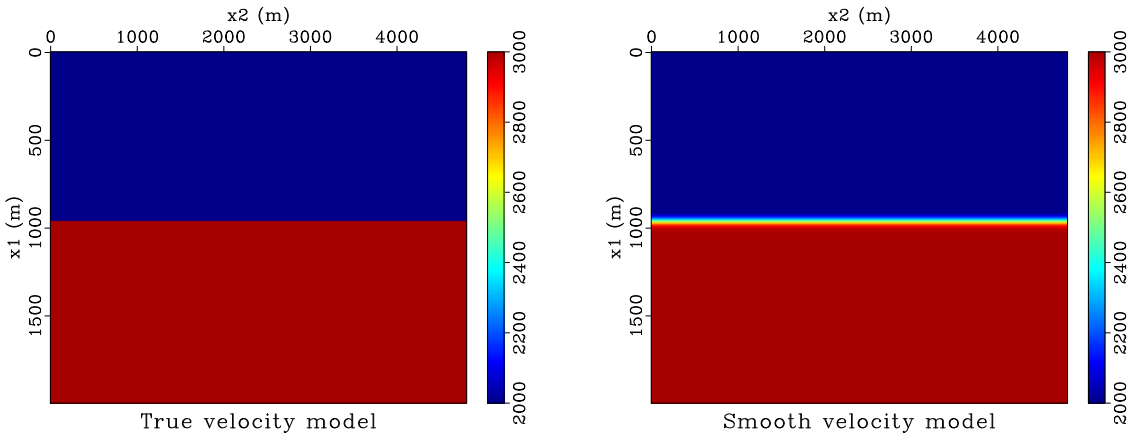

FIG. 7: (a) True horizontal-layered velocity model. (b) Smoothed horizontal-layered velocity model.

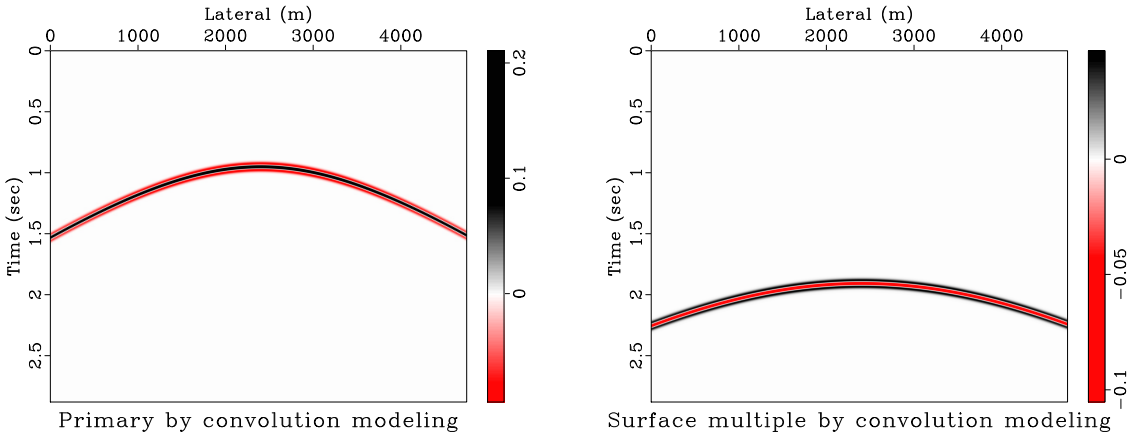

FIG. 8: (a) Primary from convolution modeling. (b) First-order surface multiple from convolution modeling.

filtering (shown in Figures 11a and b).

The RTM using the primary only (Figure 12a) shows concentrated illumination for the first horizontal layer, but poor illumination for the dipping and curve layers. On the other hand, reverse time migration of the first-order multiple (Figure 12b) expands the aperture illumination for all the layers although there are some new artifacts. It seems that the multiple also helps to enhance the vertical resolution. However, the curve reflector at the bottom in both images cannot be recovered in high quality. To improve the more in-depth structure information, next we will apply LSRTM of primary and surface multiple respectively.

In Figure 13a-b, we see results from LSRTM after five iterations. LSRTM of the surface multiple in Figure 13(b) flattens the horizontal reflector edges and also enhances the amplitude of the upper-side dipping event. The migration outcome also broadens the gentler flank information between 500-1000 meters and 4000-4500 meters offset at around 3000

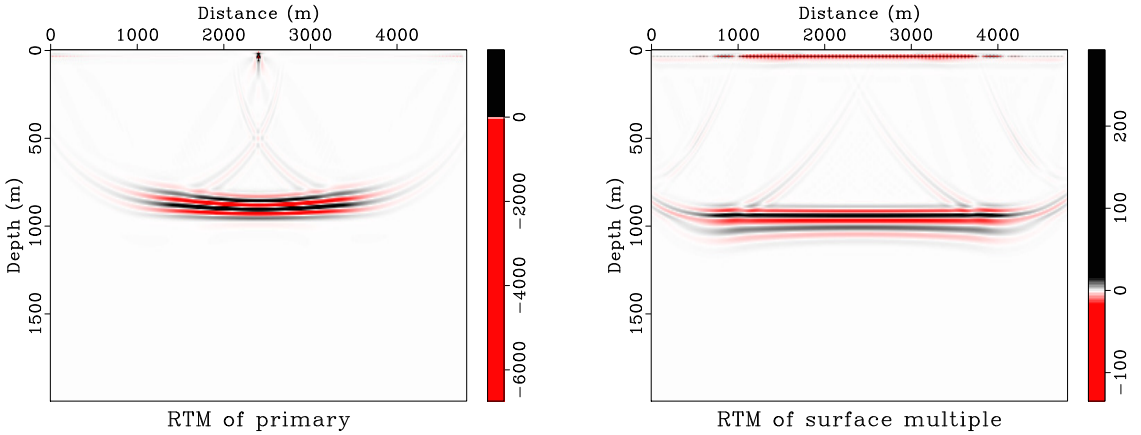

(a) (b)

FIG. 9: (a) Reverse time migration of primary reflection. (b) Reverse time migration of surface multiple.

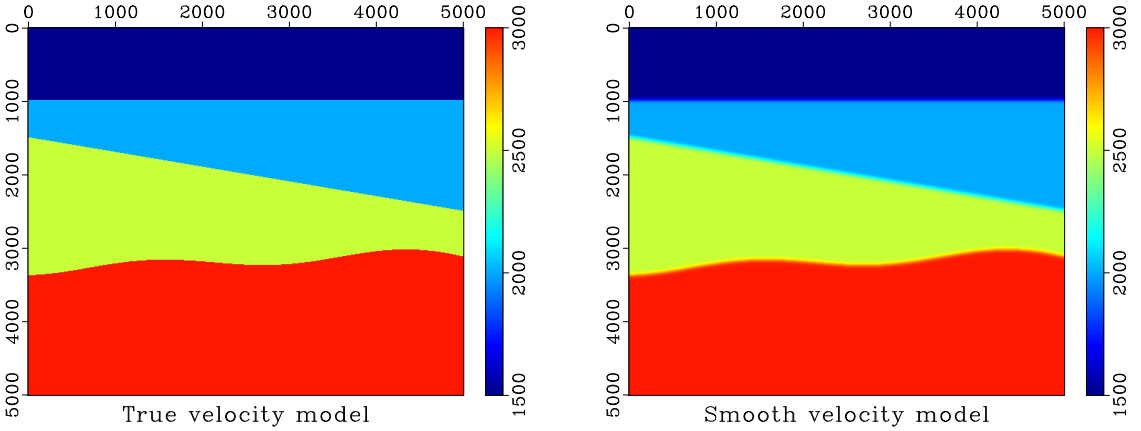

(a) (b)

FIG. 10: (a) True velocity model. (b) Smoothed velocity model.

meters depth. We expected, LSRTM would suppress these artifacts better but may need some additional constraints, which will be the topic of a future report.

Example 3: FWM and primary wavefield migration (PWM) in horizontally layered model

In this example, we will test the concept of using full wavefields including primary, surface multiple and internal multiple through FWM. Results are very preliminary and more work is required. We used a three horizontal-layer model Figure 14 in which velocities were 1500 m/s, 2000 m/s and 3000 m/s. The model size was 128 $\times$ 80 gridpoints with 5 meters as an interval. Receivers were assigned on the surface with 5 meters spacing. One source was set in the centre of the model at 20 meters in depth using a minimum phase wavelet. We simulated with finite differences a maximum time of 1.024 seconds with a sampling rate of 1 milliseconds.

We performed two experiments. Experiment 1 is using FWM with total primary and

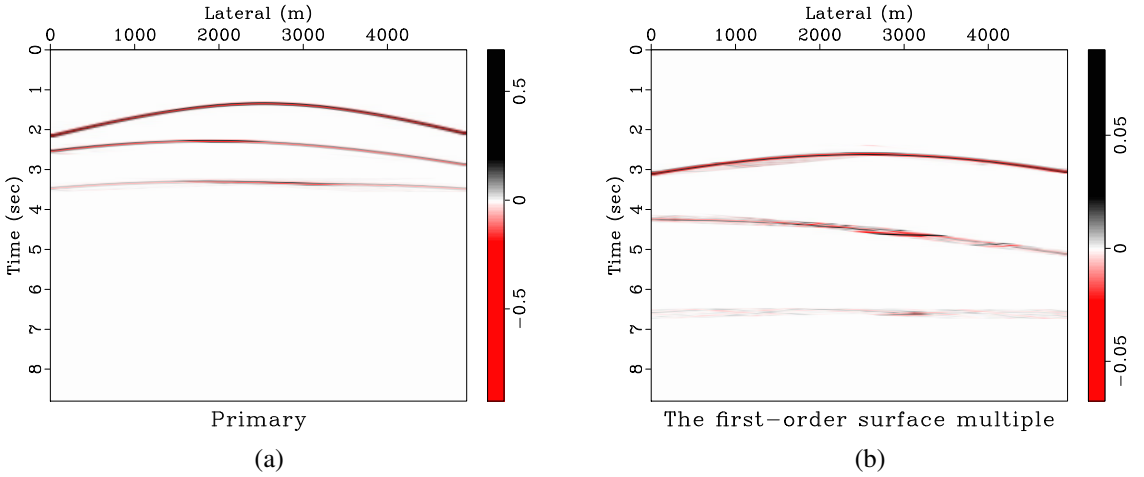

FIG. 11: (a) Primary in the shot record. (b) First-order surface multiple in the shot record.

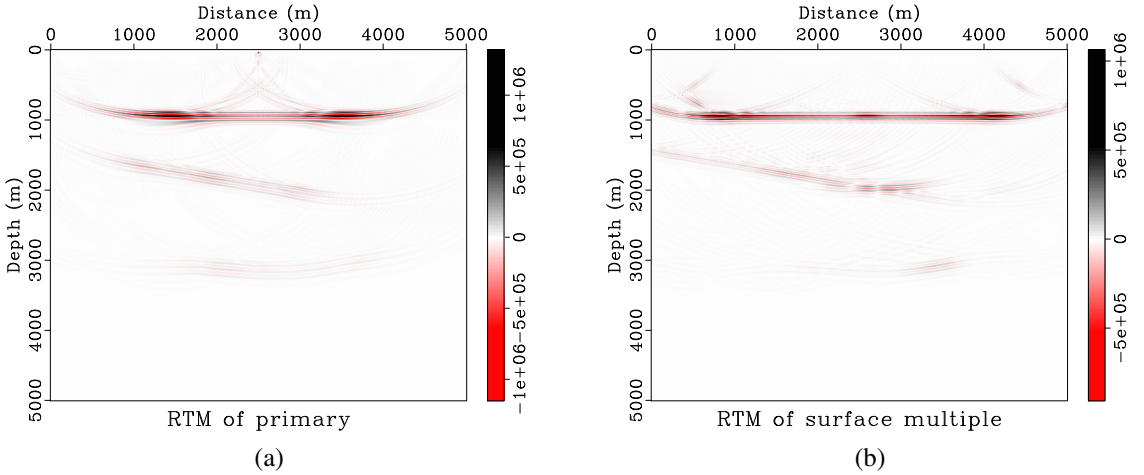

FIG. 12: (a) Reverse time migration of primary reflection. (b) Reverse time migration of surface multiple.

multiple reflections (source side: $S^+ + R^{\cap}P^-$; δS is included). The source-side includes primary and recorded surface multiples, and scattering term δS illustrates the interbed multiples. Experiment 2 is implementing PWM without surface multiple nor internal multiple reflections (source side: S^+; δS is not included). That is, in experiment 2 we only simulate impulsive wavelet on the surface to create primary reflections at the subsurface. The observation data was generated by finite-difference method with PML boundary condition (Fathalian et al., 2019).

For forward modeling, compared with the shot record (Figure 15a and blue line in Figure 16), our predicted data with total wavefields (Figure 15b and red line in Figure 16) can predict most of the seismic events and add reflections from the surface and interbedding structure. Precisely, internal multiple between two reflectors and primary from the second reflector generated by finite-difference method interference with each other at 0.406 seconds. However, forward modeling in FWM predicts those two events individually at around 0.386 and 0.429 seconds, which means full-wavefield forward modeling can provide additional reflection from the second reflector. Predicted data in experiment 2

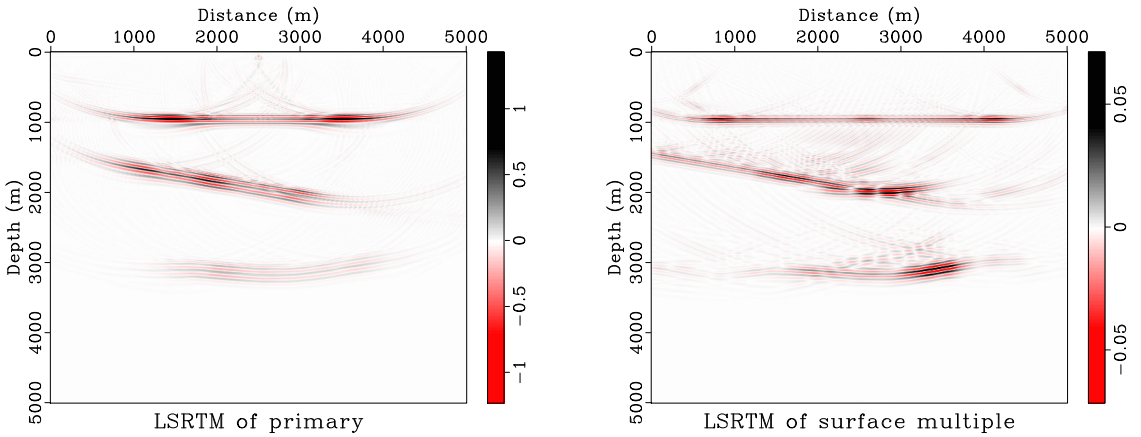

(a) (b)

FIG. 13: (a) Least-squares reverse time migration of primary reflection. (b) Least-squares reverse time migration of surface multiple.

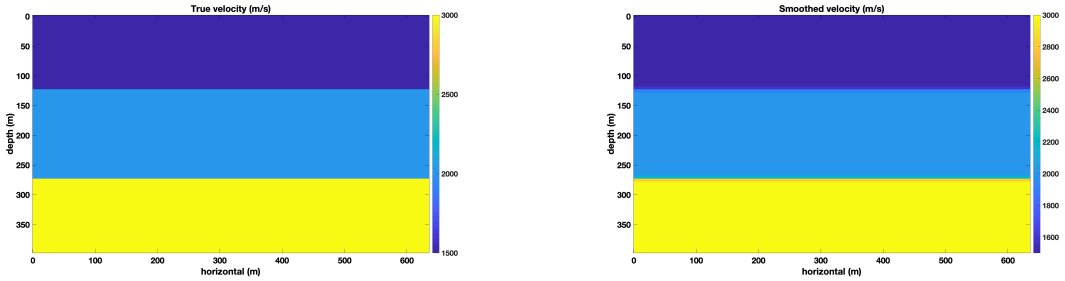

(a) (b)

FIG. 14: (a) True velocity model. (b) Smoothed velocity model.

(Figure 15c and orange line in Figure 16) generates primary only which is corresponding to observed data, whereas there is no data amplitude after 0.500 seconds compared with full-wavefield data where the surface and internal multiples should exist.

The updated reflection coefficient after using full-wavefield migration (black line in Figure 17) is more accurate and close to the true reflection coefficient values compared with applying primary only (orange line in Figure 17). Precisely, at depth 270 meters, FWM improves reflectivity coefficient amplitude and is 16.9% larger than PWM and 48.2% larger than initial model, which means FWM can provide more information from surface and internal multiples for migration. However, FWM generates some unexpected crosstalks at depth 20 and 250 meters, it might be caused by an unstable step size.

CONCLUSIONS

In this paper, we have examined two different uses of energy from multiples for migration. In the first case, we use surface multiples, in the second case, we use both surface and internal multiples.

For RTM of surface multiples, we use primaries as the injected source. In principle, using multiples would suggest a simplification of the data flow since we wouldn't need to

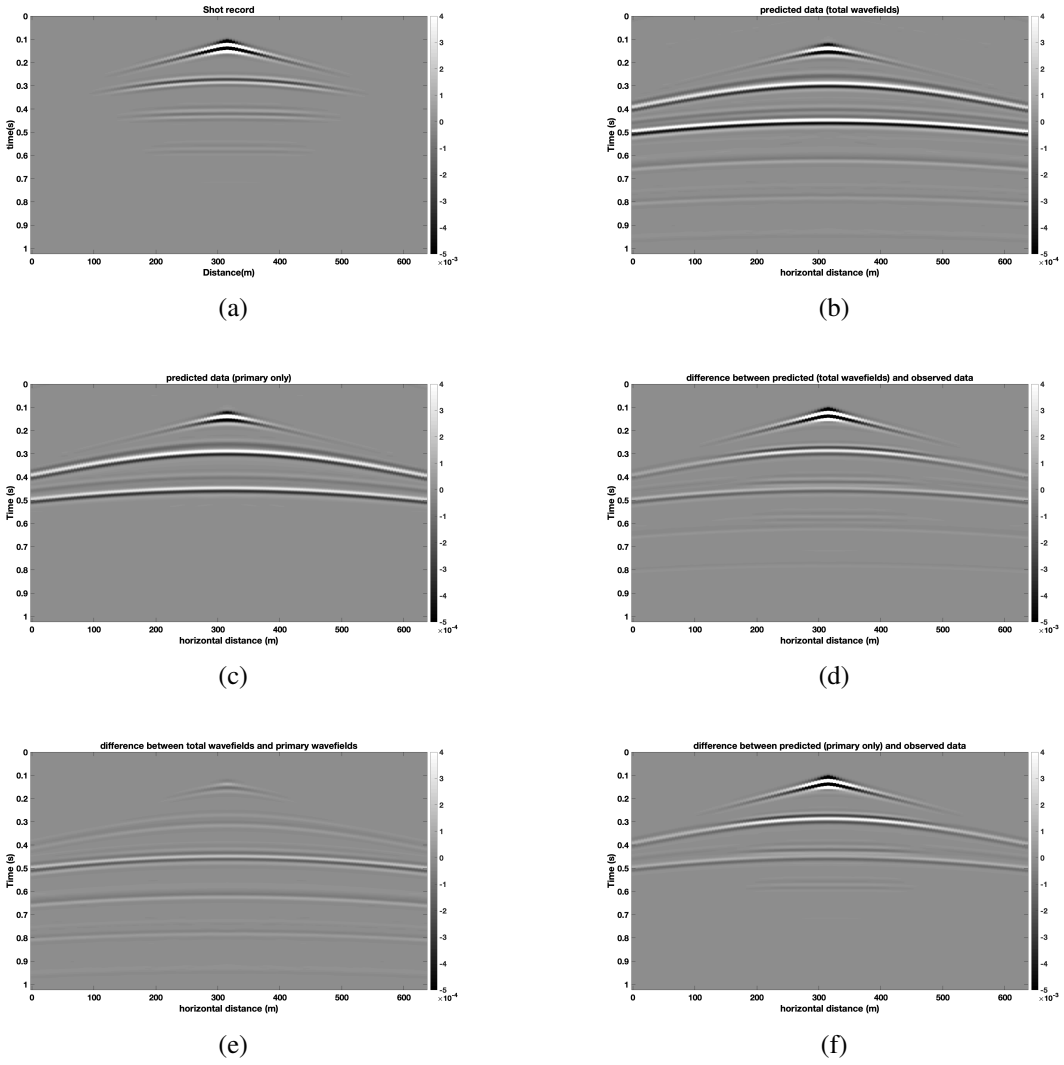

FIG. 15: (a) Observed data. (b) Predicted data with total wavefields. (c) Predicted data with primary only. (d) Difference between (a) and (b). (e) Difference between (b) and (c). (f) Difference between (a) and (c).

estimate the wavelet and attenuate multiples. In reality, however, we still need to estimate a primaries only data set to use as a source to avoid crosstalk between different orders of multiples (let us call primaries order zero multiple). The main benefit though is that migration of multiples can enhance the illumination and signal-to-noise ratio in the image as well as improve resolution.

As a further improvement, LSRTM should mitigate the inherent crosstalk and artifacts which would allow one to avoid multiple attenuation resulting in a simplified data flow. At the moment, however, we still need to separate them at front and the separation quality matters. Using surface multiples is very promising but brings some extra sensitivity on velocities forcing one to have a better background velocity model.

Although the previous approach could, in principle, be used for migration of internal multiples (if the velocity model is sharp), in practice the many orders of crosstalk make this

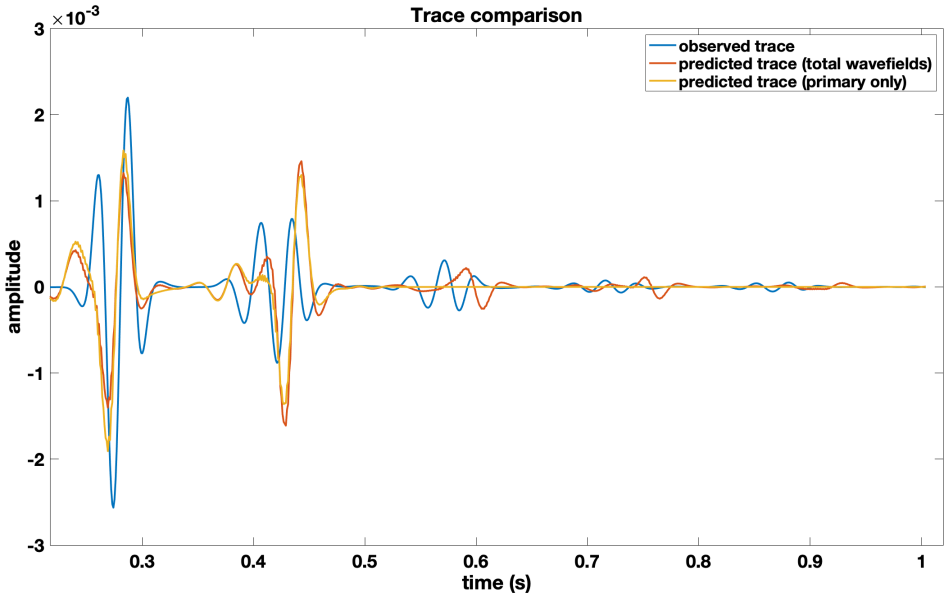

FIG. 16: Trace comparison (Trace number = 64)

very difficult. That is why FWM was proposed as a more controlled multiple integration. Now the multiples are created by explicitly adding operator components that generate them during forward and inverse propagation. Full wavefield migration is an iterative inversion-based approach that can enhance the migration accuracy by calculating corrections to existing reflector amplitudes from the primary and multiple energy. This method is a controlled approach to considering reflection and transmission energy. The number of round-trips can also be controlled. However, just as in RTM with multiples, if the background velocity model is wrong then so will be the wavefield extrapolator.

FUTURE WORK

Results shown in this report are all quite preliminary and much work is required in the future to understand these methods and make them practical. For RTM and LSRTM of surface multiples, we would like to use surface-related multiple elimination (SRME) method in more complex settings to obtain good estimates of primaries and multiples. We have tried Radon transform in this work, which is better for attenuating than to separating multiples. Also, amplitude compensation and divergence should be considered for recovering the amplitude from deeper reflectors. For the FWM approach, we have just scratched the surface. We need to work on the iterative approach and in F-X operators to account for lateral velocity variations.

ACKNOWLEDGEMENTS

The authors would like to thank the sponsors of CREWES for continued support. This work was funded by CREWES industrial sponsors, China Scholarship Council (CSC), and NSERC (Natural Science and Engineering Research Council of Canada) through the grant CRDPJ 461179-13. We also thank Dr. Mikhail Davydenko, Dr. Samuel Gray, Dr. Jian Sun and Dr. Alison Malcolm for valuable discussions, and Dr. Ali Fathalian for his finite-

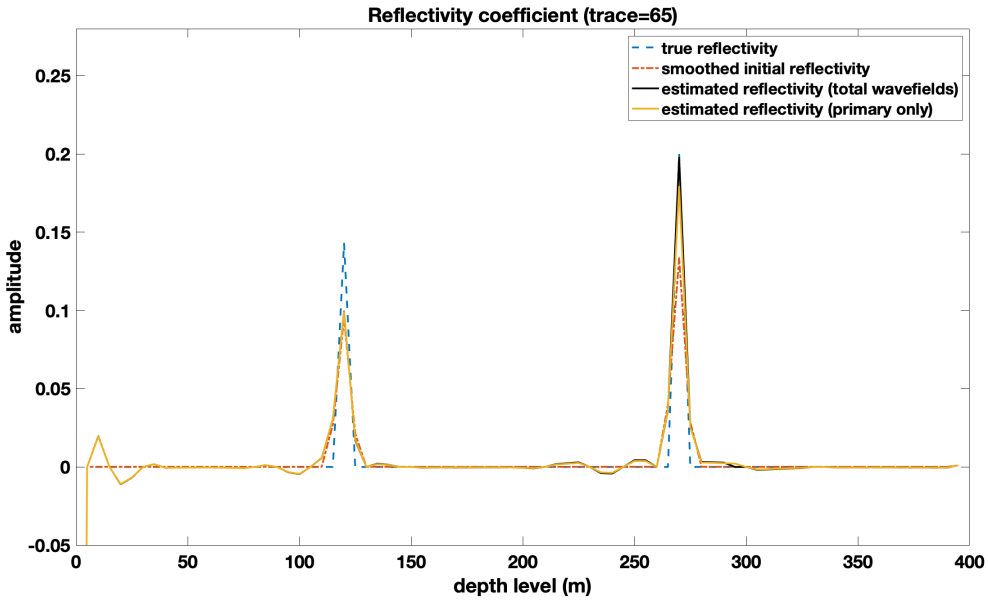

FIG. 17: Reflectivity coefficient comparison (Trace number = 64)

difference forward modeling code with PML boundary condition.

REFERENCES

Amundsen, L., 1991, Comparison of the least-squares criterion and the cauchy criterion in frequency-wavenumber inversion: Geophysics, **56**, No. 12, 2027–2035.

Atkinson, F., 1960, Wave propagation and the bremmer series: Journal of Mathematical Analysis and Applications, **1**, No. 3-4, 255–276.

Baysal, E., Kosloff, D. D., and Sherwood, J. W., 1983, Reverse time migration: Geophysics, **48**, No. 11, 1514–1524.

Berkhout, A., 2014, Review paper: An outlook on the future of seismic imaging: Part II: Full-wavefield migration: Geophysical Prospecting, **62**, 931–949.

Berkhout, A., De Vries, D., Baan, J., and Van den Oetelaar, B., 1999, A wave field extrapolation approach to acoustical modeling in enclosed spaces: The Journal of the Acoustical Society of America, **105**, No. 3, 1725–1733.

Berkhout, A., and Verschuur, D., 1994, Multiple technology: Part 2, migration of multiple reflections: 64th annual international meeting, seg, expanded abstracts, 1497–1500.

Berkhout, A., and Verschuur, D., 2016, Enriched seismic imaging by using multiple scattering: The Leading Edge, **35**, No. 2, 128–133.

Bremmer, H., 1951, The wkb approximation as the first term of a geometric-optical series: Communications on pure and applied mathematics, **4**, No. 1, 105–115.

Davydenko, M., and Verschuur, D., 2017, Full-wavefield migration: Using surface and internal multiples in imaging: Geophysical Prospecting, **65**, No. 1, 7–21.

Fathalian, A., Trad, D. O., and Innanen, K. A., 2019, An approach for attenuation-compensating multidimensional constant-q viscoacoustic reverse time migration: Geophysics, **85**, No. 1, 1–57.

Gazdag, J., and Sguazzero, P., 1984, Migration of seismic data by phase shift plus interpolation: Geophysics, **49**, No. 2, 124–131.

Guitton, A., 2002, Shot-profile migration of multiple reflections, *in* SEG Technical Program Expanded Abstracts 2002, Society of Exploration Geophysicists, 1296–1299.

Liu, Y., Chang, X., Jin, D., He, R., Sun, H., and Zheng, Y., 2011, Reverse time migration of multiples for subsalt imaging: Geophysics, **76**, No. 5, WB209–WB216.

Liu, Y., Liu, X., Shao, Y., Osen, A., Zheng, Y., and Hu, H., 2016, Least-squares reverse time migration of controlled order multiples, *in* SEG Technical Program Expanded Abstracts 2016, Society of Exploration Geophysicists, 4240–4244.

Lu, S., Liu, F., Chemingui, N., Valenciano, A., and Long, A., 2018, Least-squares full-wavefield migration: The Leading Edge, **37**, No. 1, 46–51.

Mendel, J. M., 1978, Bremmer series decomposition of solutions to the lossless wave equation in layered media: IEEE Transactions on Geoscience Electronics, **16**, No. 2, 103–112.

Sengbush, R. L., 1983, Seismic exploration methods: Springer, Dordrecht.

Snieder, R., 2002, Elastic coda wave interferometry, a new tool for the instrumented oilfield, *in* SEG Technical Program Expanded Abstracts 2002, Society of Exploration Geophysicists, 1650–1653.

Verschuur, D., and Berkhout, A., 2011, Seismic migration of blended shot records with surface-related multiple scattering: Geophysics, **76**, No. 1, A7–A13.

Verschuur, D., and Berkhout, A., 2015, From removing to using multiples in closed-loop imaging: The Leading Edge, **34**, No. 7, 744–759.

Zhang, D., and Schuster, G. T., 2013, Least-squares reverse time migration of multiples: Geophysics, **79**, No. 1, S11–S21.